Advances in Capacitive, Eddy Current, and Magnetic Displacement Sensors and Corresponding Interfaces

George, Boby; Tan, Zhichao; Nihtianov, Stoyan

DOI
10.1109/TIE.2017.2726982

Publication date
2017

Document Version
Final published version

Published in
IEEE Transactions on Industrial Electronics

Advances in Capacitive, Eddy Current, and Magnetic Displacement Sensors and Corresponding Interfaces

Boby George, *Member, IEEE*, Zhichao Tan, *Member, IEEE*, and Stoyan Nihtianov, *Senior Member, IEEE*

***Abstract*—This paper presents a review of the latest advances in the field of capacitive, inductive (eddy current), and magnetic sensors, for measurement of absolute displacement. The need for accurate displacement and position measurement in the micrometer, nanometer, and subnanometer scales has increased significantly over the last few years. Application examples can be found in high-tech industries, metrology, and space equipment. Besides measuring displacement as a primary quantity, absolute displacement sensors are also used when physical quantities such as pressure, acceleration, vibration, inertia, etc., have to be measured. A better understanding of the commonalities between capacitive, inductive, and magnetic displacement sensors, as well as the main performance differences and limitations, will help one make the best choice for a specific application. This review is based on both theoretical analysis and experimental results. The main performance criteria used are: sensitivity, resolution, compactness, long-term stability, thermal drift, and power efficiency.**

***Index Terms*—Capacitive sensors, displacement, eddy current sensors, magnetic sensors.**

I. Introduction

A COMMON feature of capacitive, inductive (eddy current), and magnetic displacement sensors is that they all use specific aspects of the electromagnetic field to convert displacement into an electrical signal. Unlike incremental sensors (e.g., encoders, interferometers), these sensors can measure the absolute position of a target (with respect to the reference). Over the last decade, extensive research work has been conducted on these types of displacement sensors, with this main objective: to enhance performance with respect to sensitivity, resolution, compactness, long-term stability, thermal drift, and the power efficiency of the electronic interface [1]–[15]. The growth in the industrial and consumer sensing applications opened-up new requirements and challenges for displacement sensors; not just in the nanometer regime [1], [2], but in the micrometer and wider-range (few cm) position sensors [3] with nanometer precision [6]. Energy consumption reduction of these sensor systems is a steady trend in the past few years, related to the integration of the interface electronics together with the sensing element into one body without causing self-heating, and allowing the realization of wireless sensor networks with long life local power supply using batteries and/or energy harvesting [7], [9]. Being reactive components, the sensing elements in capacitive and eddy current sensors consume very little energy. However, the interface electronics needs to compromise between the performance and the power consumption. This is driving the competition in the field of power-efficient sensor interface electronics for this type of sensors [2], [4], [5]. Thus, in this review paper, a clear emphasis is given on analysis of the various recently reported promising interface principles. The solid-state magnetic field sensors and related applications attract a growing interest in the displacement domain, owing to number of advantages such sensors possess. The last section of the paper is devoted to review of those types of sensors to assess the state of the art and to explore the future possibilities. The ambition of this paper is to present the latest advances in the field, in the above-mentioned characteristics. The paper is organized into three main sections, corresponding to the sensors of interest: capacitive, eddy current, and magnetic sensors.

Manuscript received November 28, 2016; revised March 4, 2017, April 23, 2017, and May 20, 2017; accepted June 4, 2017. Date of publication July 13, 2017; date of current version October 24, 2017. *(Corresponding author: Zhichao Tan.)*

B. George is with the Electrical Engineering Department, Indian Institute of Technology Madras, Chennai 600036, India (e-mail: boby@ee.iitm.ac.in).

Z. Tan is with Analog Devices Inc., Wilmington, MA 01887 USA (e-mail: Zhichao.Tan@analog.com).

S. Nihtianov is with ASML, Veldhoven 5504 DR, The Netherlands, and also with the Technical University in Delft, Delft 2628 CD, The Netherlands (e-mail: S.Nihtianov@TUDelft.nl).

Color versions of one or more of the figures in this paper are available online at http://ieeexplore.ieee.org.

Digital Object Identifier 10.1109/TIE.2017.2726982

II. Capacitive Displacement Sensors and Interfacing

Capacitive linear and angular displacement sensors have been widely used in industrial applications for many decades now. Most micro-electromechanical systems (MEMS) inertial sensors belong to this category since they rely on the same principle: sensing the change in position of a proof mass resulting from acceleration or rotation. Capacitive sensors are quite attractive as they are easy to manufacture and their power consumption is extremely small [3]. Thus, they are a good candidate for applications where power efficiency is important [4], [5].

In this section, we first discuss the capacitive position sensing principle, since the interface/readout circuit design depends highly on the properties and structure of the sensing element. Next, we review several sensor interfacing techniques. Since

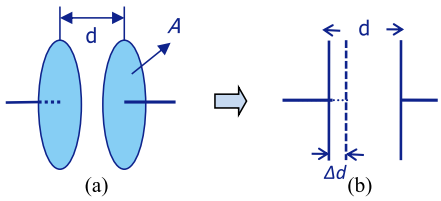

Fig. 1. (a) A parallel-plate capacitive position sensor and (b) working principle [2].

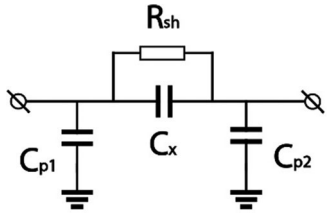

Fig. 2. Electrical model of a capacitive sensor [4].

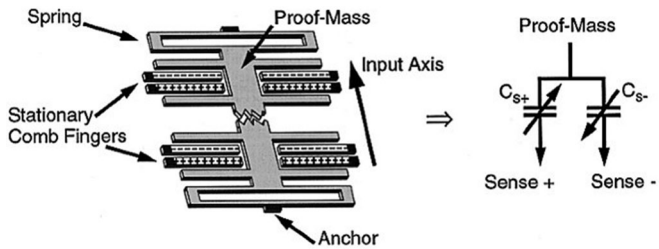

Fig. 3. Differential capacitive acceleration sensing element [22].

nowadays data processing is performed in the digital domain, we mainly focus on interfaces which convert capacitance into a digital code. These types of interfaces are referred as "capacitance-to-digital converters" (CDCs). Two types of CDCs are discussed: indirect CDCs and direct CDCs. Indirect CDCs use an independent functional block to convert capacitance into an analog signal such as voltage, current, time/frequency, and then digitize that analog signal. Direct CDCs combine both functions in one functional block by using a charge-balancing technique to compare the value of the unknown sensing capacitor to a reference capacitor. Both interface types will be discussed in detail.

A. Capacitive Position Sensing Element

A capacitive displacement sensor can be build either with discrete components [16]–[18] or by using MEMS technology [19]–[22]. A parallel plate capacitor is shown in Fig. 1 [2].

The capacitance of this simple parallel-plate structure can be calculated using the following simplified equation (without considering the fringe effects of the electric field, the surface quality of the plates, and the possible tilt between them):

$$C = \varepsilon \frac{A}{d} \tag{1}$$

where A is the area and d is the distance between the two parallel plates, and ε is the dielectric constant of the material between the two plates. The changes in both A and d can be used to sense the displacement. For typical geometries and small displacement range, the gap variation is preferred as it is much smaller than the overlap and hence provides higher sensitivity:

$$\frac{\Delta C}{\Delta d} = -\varepsilon \frac{A}{d^2}. \tag{2}$$

The higher sensitivity, however, comes at the cost of nonlinearity which is normally accounted for by backend processing. Equation (2) shows that the sensitivity of the capacitive position sensor is inversely proportional to the square of the distance. For this reason MEMS inertial sensors usually have a gap of only a couple of micrometers between the sense and the fixed fingers to maximize the sensitivity of the sensor [20]. Independent of the specific design, capacitive sensors can always be represented with a two-terminal electrical model, as shown in Fig. 2 [4].

One of the challenges for capacitive sensor interfaces is the small capacitance variation being only a fraction of the sensor capacitance. This is one important reason why CDCs cannot compete with analog-to-digital converters (ADC) with respect to power efficiency, despite the similarity in topology [4], [5], [23]. The parasitic capacitances at the two terminals of the sensing capacitor cause similar limitations and errors, as their value is often comparable to, or even larger than the measured capacitance. This introduces additional requirement for the interface electronics, i.e., the output signal of the interface should be made insensitive to the parasitic capacitance and maximized with respect to the change in the sensor capacitance.

A differential structure for the capacitive sensor is preferred due to the efficient elimination of external interferences. This also allows the use of a much more stable differential interface circuit topology. In many cases, the differential capacitive sensor consists of three electrodes and hence has three terminals comprising two capacitors with one common electrode. This three-terminal structure is popular in MEMS accelerometers (see Fig. 3) [22]. The capacitance variation can be calculated as

$$\begin{aligned} \Delta C &= C_{x1} - C_{x2} \\ &= \varepsilon \frac{A}{d + \Delta d} - \varepsilon \frac{A}{d - \Delta d} \\ &= -\varepsilon \frac{A 2 \Delta d}{d^2 - \Delta d^2} \\ &\approx -C_0 \frac{2\Delta d}{d}. \end{aligned} \tag{3}$$

B. Indirect Capacitance-to-Digital Converter

In indirect CDCs, the capacitance of the capacitive displacement sensors is first converted into voltage [4], [24]–[26] or a time interval [27]–[31], and then digitized with an ADC or time-to-digital converter (TDC). In some cases, additional modulation blocks and anti-aliasing filters are required [24], [25]. Fig. 4 shows a functional diagram of the indirect CDC.

Since ADCs and TDCs are considered standard building blocks in this design, here we focus on how capacitance is converted into voltage or time. A switched capacitor charge amplifier (CA) can be used to convert capacitance into voltage, due to its discrete time nature. Fig. 5 shows a CA for a

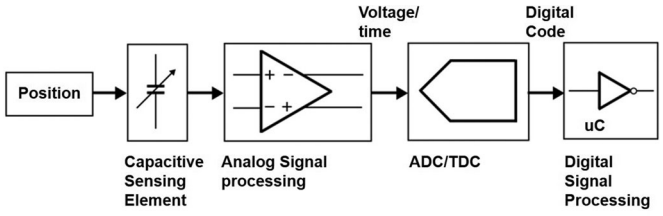

Fig. 4. Capacitance-to-voltage/time-to-digital converter.

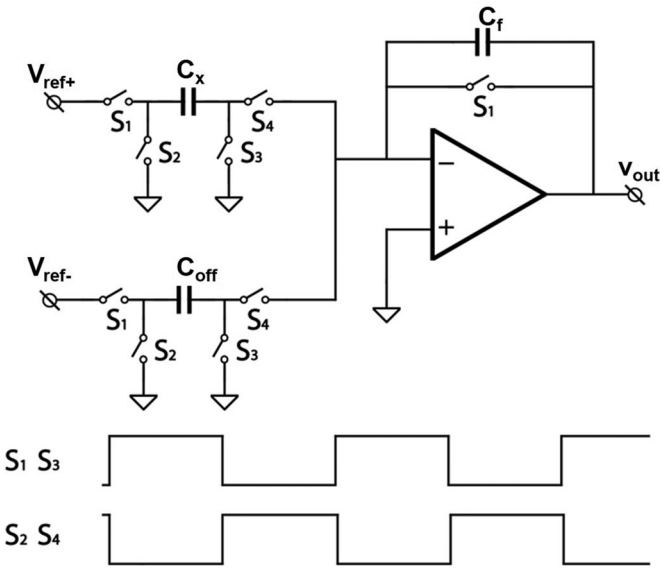

Fig. 5. Charge amplifier for the single-ended sensor.

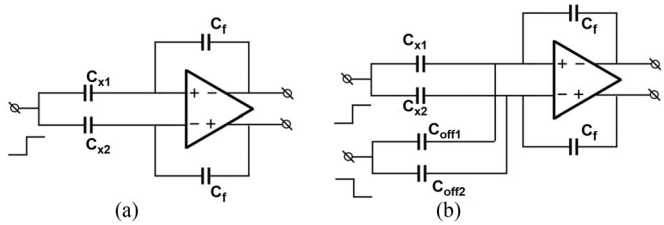

Fig. 6. Middle electrode drive scheme: (a) conceptual idea and (b) with common mode correction.

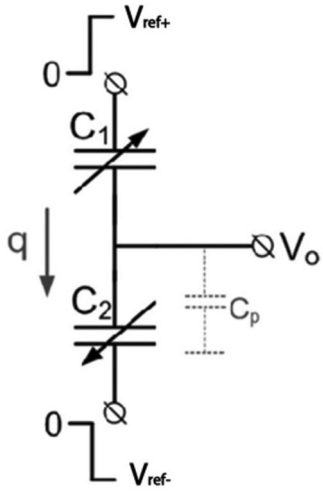

Fig. 7. Middle electrode sense scheme [21].

single-ended sensor represented by a two-terminal sensing capacitor C_x. As mentioned in Section II-A, the sensing elements have a relatively large baseline (offset) capacitance which should be cancelled before the capacitance-to-voltage conversion to maximize the usage of the operational transconductance amplifier (OTA) output swing. $C_{\rm off}$ can be used for the baseline capacitance cancelation [32]. If the dc gain of the CA is large enough, the negative input of the OTA can be treated as virtual ground, maintaining the charge of the parasitic capacitance close to zero in any of the operation phases.

The output voltage of the CA is

$$V_{\rm out} = V_{\rm ref}\frac{C_x - C_{\rm off}}{C_f} = V_{\rm ref}\frac{\Delta C_x}{C_f}. \tag{4}$$

As shown in (4), only the changing part of the sensing capacitance is converted. To track a possible variation in the sensor baseline capacitance, the offset capacitor can be made programmable [33].

A fully differential readout structure is usually preferable for its superior performance against interference and circuit supply noise. The fully differential sensing element can be realized with two separate sensing elements [32], [33] or with a three-terminal structure [22], [24], as presented in the previous section. For a three-terminal device, there are basically two ways to drive the sensing elements to obtain a position-modulated capacitance: with a middle electrode drive (MED) or middle electrode sensing scheme. The MED scheme benefits from inherent fully differential reading, as shown in Fig. 6(a). The switches are omitted for simplicity [25], [30]. The excitation signal drives the middle electrode. The output voltage of the CA is

$$V_{\rm out.diff} = V_{\rm ref}\frac{C_{x1} - C_{x2}}{C_f} = V_{\rm ref}\frac{\Delta C_x}{C_f} \tag{5}$$

$$V_{\rm out.comm} = V_{\rm ref}\frac{C_{x1} + C_{x2}}{2C_f} \tag{6}$$

where $V_{\rm out.diff}$ and $V_{\rm out.comm}$ represent the differential and the common mode portion of the output voltage. There is one drawback of the diagram shown in Fig. 6(a): the drive signal applied to the middle electrode can cause a large output common voltage step, which is given in (6). Due to this large output common mode voltage shift, the amplifier requires a large output common mode swing, which complicates the design and leads to higher power consumption. It also puts pressure on the preceding stages since they have to take care of this common mode voltage shift. This problem can be resolved by introducing an offset capacitor [see Fig. 6(b)] in a similar way, as already presented in Fig. 5.

Alternatively, the middle electrode can be connected to the CA input. This approach is popular in MEMS position sensing applications. Complementary excitation signals drive the other two electrodes, as shown in Fig. 7 [21].

An important advantage of the "middle electrode" sensing principle is the possibility for a linear transfer function [21]. If all electrodes in Fig. 7 are reset to ac ground and two complementary drive signals are applied to the drive electrodes, the

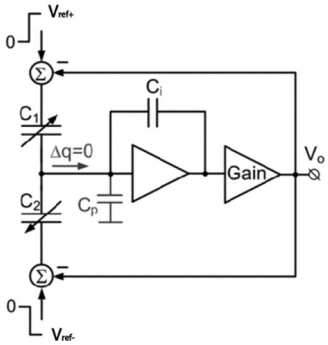

Fig. 8. Charge balanced capacitance-to-voltage converter [21]. V_o is the output voltage.

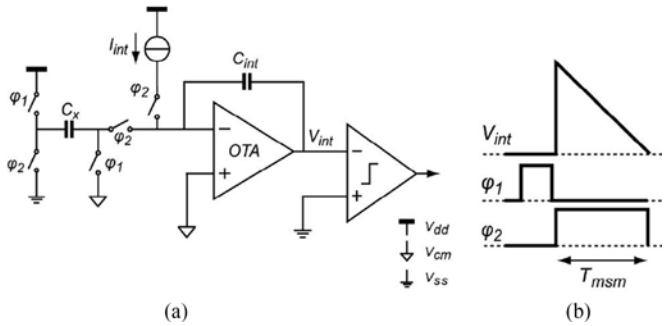

Fig. 9. Simple capacitance-to-time converter: (a) circuit and (b) timing diagram [28].

output voltage $V_{\rm out}$ will be

$$V_{\rm out} = V_{\rm ref}\frac{C_{x1} - C_{x2}}{C_{x1} + C_{x2}} = V_{\rm ref}\frac{\Delta d}{d_0}. \tag{7}$$

This linear relationship is valid if there is a perfect charge balance between the two capacitors (C_1 and C_2) so that there is no charge flowing to the input of the CA, which unfortunately is not the case with the circuit in Fig. 5. The balance can be achieved by introducing a mismatch between the magnitudes of the excitation signals. For this, the idea used in the capacitance-to-voltage converter scheme shown in Fig. 8 [21] can be explored. When the measurand is not zero, the feedback loop, including the sensors and the CA, will automatically adjust the amplitudes of the excitation voltages applied to the sensor capacitances C_1 and C_2 such that it ensures the corresponding two charges Q_{c1} and Q_{c2} always remain equal and the resulting difference charge Δq is kept close to zero.

There are many circuit topologies reported which transfer the output of the capacitance-to-time period to the TDC for further processing to obtain a digital output [27], [31]. In all of them, the unknown capacitance is charged by a controlled current source $I_{\rm int}$. A simple capacitance-to-time converter, referred to as a "period modulator," is shown in Fig. 9 [28]. The time period $T_{\rm msm}$ indicated in Fig. 9 can be calculated in terms of the power supply voltage $V_{\rm dd}$ and sensor capacitance C_x using

$$T_{\rm msm} = \frac{V_{\rm dd}}{I_{\rm int}}C_x. \tag{8}$$

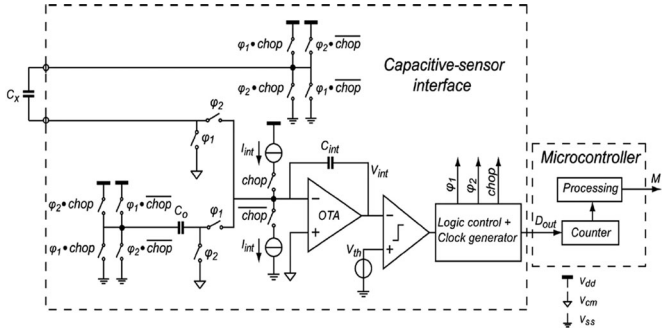

Fig.10. Example of a capacitance-to-period modulator [29].

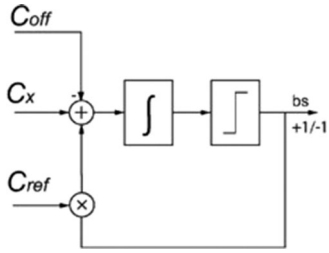

Fig.11. Example of a CDC based on a first-order charge-balancing delta sigma modulator [32].

The circuit shown in Fig. 9 can be made self-oscillating, as shown in Fig. 10. The presented relaxation oscillator generates time intervals proportional to the unknown capacitance C_x [27], [28].

The period modulator operates without an external clock due to its asynchronous nature. Chopping and autocalibration techniques can be applied to improve its performance [28]. The measurement results reported in [28] show that the interface achieves 15-bit resolution with input range up to 6.8 pF, while consuming 64 μA from a 3.3-V supply. The measurement time is 7.6 ms.

C. Direct Capacitance-to-Digital Converter

Direct CDCs convert the capacitance into digital code primarily using the "charge balancing" technique. Charge balancing can be implemented using: delta sigma modulation, a successive approximation register technique, or a single/multislope technique. This section will focus on these three techniques [32]–[37].

Fig. 11 shows an example of a CDC based on a first order charge-balancing delta sigma modulator [32]. It also compensates the baseline capacitance of the sensing element with $C_{\rm off}$, using the same technique described previously. In every clock cycle, a charge $V_{\rm ref}(C_x - C_{\rm off})$ is added to the integrator. The reference capacitor adds or subtracts a charge $V_{\rm ref}C_{\rm ref}$ to or from the integrator. After N clock cycles, the negative feedback ensures that the charge from the sensing capacitor will be balanced by the charge delivered by the reference capacitor [32]:

$$(C_x - C_{\rm off}) - \mu \cdot C_{\rm ref} + (1-\mu)C_{\rm ref} = 0 \tag{9}$$

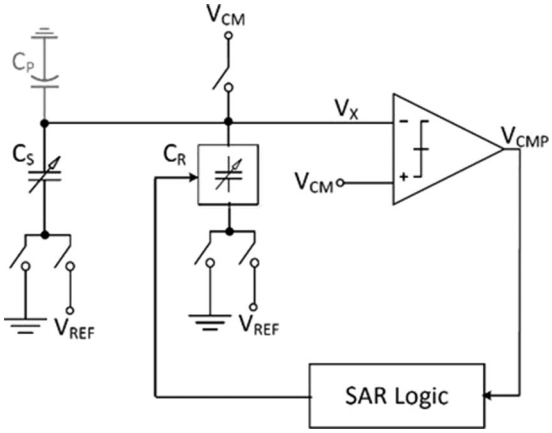

Fig. 12. Block diagram of the SAR-based CDC in [35].

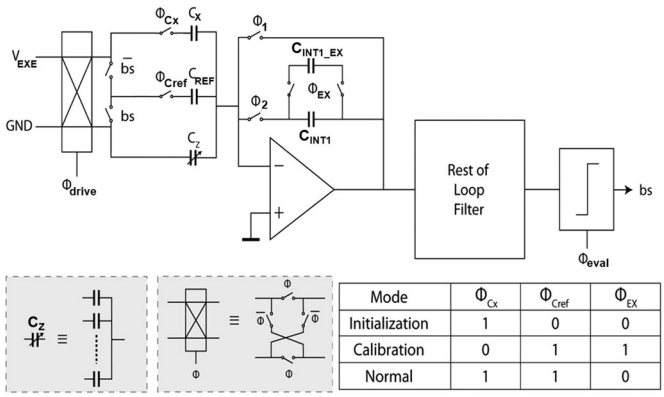

Mode	Φ_{Cx}	Φ_{Cref}	Φ_{EX}
Initialization	1	0	0
Calibration	0	1	1
Normal	1	1	0

Fig. 13. Example of an SAR-based CDC [37].

where μ is the bit density of the bit-stream. The sensing capacitance is calculated with the following equation:

$$C_x = C_{\text{ref}}(2\mu - 1) + C_{\text{off}}. \tag{10}$$

The conversion time of the delta-sigma modulator-based CDC can be reduced by increasing its order (i.e., using more than one integrator in the loop) without changing the quantization requirement [32]. CDCs based on the sigma-delta modulation are available in the market, e.g., AD7745 is a 24 bit CDC (21 effective bit resolution) with an accuracy of $\pm$ 4 fF and nonlinearity of 0.01%. Such ICs are quite useful for building standalone measurement systems for capacitive sensors within the range of $\pm$4 pF. There is also low power sigma-delta modulation-based CDC available, such as AD7151 which only consumes 70 μA while provide 12-bit resolution.

Successive-approximation-register (SAR) ADCs have attracted attention due to their simple implementation and excellent energy efficiency. The SAR-based CDC shares a similar structure with the SAR ADC [35], [36]. An example of an SAR-based CDC is shown in Fig. 12.

First, the reference voltage is sampled by C_s. Next, the input node is driven to the negative reference voltage, resulting in a voltage step at the input of the comparator V_x. The SAR logic drives the digital-to-analog converter (DAC) capacitor C_R to bring V_x back to its previous level. Due to the charge-balancing principle, after the conversion, the state of the SAR logic is a digital representation of the ratio between the sensing capacitor and the reference capacitor. In SAR-based CDCs, there is usually only one active building block: a comparator. The rest of the system is implemented using switches and capacitors, making it highly energy efficient. However, due to the limited matching of the capacitors in the capacitive DAC, and the noise constraint, this type of CDC demonstrates a limited dynamic range of around 12 bits. This interface consumes 91 μA from a 3.3-V supply, and provides 12.5-bit resolution. The capacitance input range is up to 16 Pf and the measurement time is 0.65 ms.

A hybrid CDC with greater energy efficiency and resolution is reported in [37]. The combination of delta sigma modulation and the successive approximation register scheme can help the CDC benefit from the advantages of both techniques. This leads to an even more energy-efficient solution. Fig. 13 shows the functional diagram of a CDC with the "zoom in" technique, which combines delta sigma modulation and the SAR scheme. It is, basically, a charge-balancing delta sigma modulator using the SAR scheme to dynamically control the cancelation of the offset capacitor. This design achieves fast conversion time of 0.02 ms. The current consumption was 3.1 Ma from a 3.3-V supply. It also provides 17.2 bits resolution.

TABLE I
SUMMARY OF CAPACITIVE SENSOR INTERFACES

	Power, μW	Meas. Time, ms	Dynamic range, bits	Cap. range, pf
[4]	10.2	100	9	2.1–2.9
[27]	7000	100	16	~4.7
[28]	211.2	7.6	15	~6.8
[30]	15840	0.05	8.8	0.8–1.2
[31]	84	0.033	8	0.5–0.76
[32]*	10.32	0.8	12.5	0.54–1.06
[33]*	10.53	10.2	13	0.4–1.2
[34]*	0.112	6.4	7	5.3–30.7
[35]*	300.3	0.65	12.5	~16
[36]*	3.84	0.042	11.8	~16.14
[37]*	10230	0.02	17.2	~10 p
AD7745[1]	1890	11	21	−4 to 4
AD7151[1]	189	10	12	0–13

[1]Commercial products via www.analog.com.
*Interfaces of direct type (CDC).

Table I presents the summary of capacitive sensor interfaces which can be used for capacitive sensors in displacement sensing. It is difficult to choose the "best" topology over others as the choice of topology is usually application driven and specification dependent. "Indirect" interface topology usually has more flexible system design and it can be easily reconfigured to handle large variety of sensors. "Direct" type of interfaces usually results in compact system design, which makes it more suited for low power applications.

III. Eddy Current Displacement Sensors

The operation principle of eddy current sensors (ECSs) can be explained by the effect of a conductive object on the inductance of a coil through which alternating current is running.

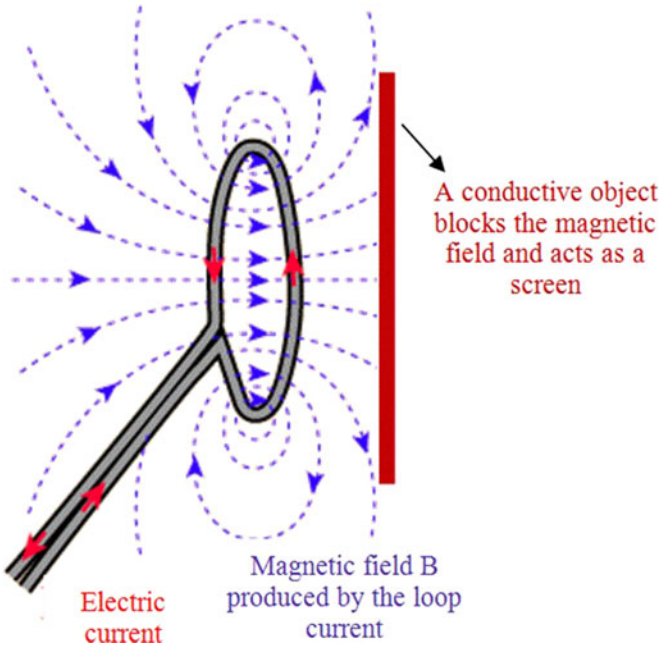

Fig. 14. Magnetic field B (dashed lines) created by an electric current through a loop.

Fig. 14 shows the lines of a magnetic field created by a current through a loop. Note that the magnetic field line trajectory is closed around the current loop which creates the magnetic field. The magnetic field lines are canceled when they cross a conductive object (the sensor target). This happens due to a secondary magnetic field with the opposite polarity that is created by the eddy currents generated in the target by the primary magnetic field. The eddy currents flow along a closed trajectory in a similar way to the primary current flowing in the loop. This phenomenon is explained by the Lorentz law for the electromagnetic-field force exerted on the point charges (free electrons) comprising the eddy currents. The sensitivity of an ECS to the position of a conductive target is based on the interaction between the primary magnetic field and the secondary magnetic field. The closer the target to the sensing coil, the stronger the magnetic field interaction. As a result, a magnetic coupling appears between the sensor and the target [6].

The displacement of the target causes the magnetic field, as well as the equivalent impedance of the coil, to change. Since magnetic fields are not sensitive to the presence of nonconductive contaminants such as oil, dirt, dust, vapor, etc., ECSs operate well even in polluted and harsh environment [8].

A. ECS Sensing Coil

Attempts to express the ECS displacement-inductance transfer function analytically are reported in [8]–[11]. However, since many parameters contribute to these analyses, the end result is always very complicated mathematics that is difficult to use in practical applications [12]. For practical assessment purposes, it is useful to approximate the ECS transfer characteristic with an exponential curve, as is done in [6]. A graphic presentation of the highly nonlinear transfer characteristic is shown in Fig. 15.

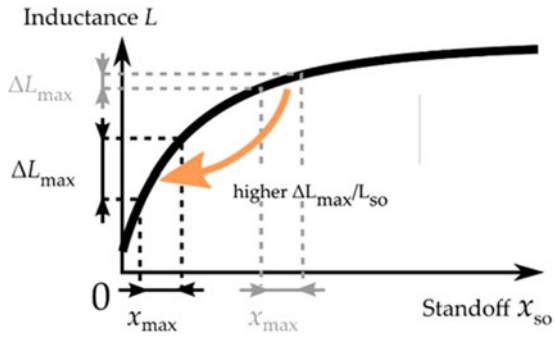

Fig. 15. Typical transfer characteristic $L(x)$ of an ECS, showing the difference in the maximum variation of the inductance $\Delta L_{\max}$, for the same displacement $x_{\max}$, at different standoff distances.

This type of ECS behavior means that sensitivity drops very quickly with increasing standoff distance from the target, similar to capacitive sensors. For a reasonable level of sensitivity it is recommended, as a rule of thumb, to limit the maximum standoff distance between the sensing coil and the target so as not to exceed 1/3 of the coil's diameter. It is important to mention that by increasing the diameter of the coil, larger standoff distances can be tolerated with the same sensitivity. However, when very small displacements have to be measured within a small displacement range, the standoff appears as a large offset in inductance, which unnecessarily increases the dynamic range for the readout electronics.

The effect of tilt (i.e., nonparallelism between the target and the sensing coil) on ECS performance is considered similar to capacitive displacement sensors with two parallel plates. Hence, for both types of sensors it is very important to align them accurately with the target. This is even more important when the ECS operates at a small standoff from the target, compared with the diameter of the sensing coil. The tilt causes deviation from the normal transfer characteristic of the sensor, and hence the measurement errors. Investigations into the tilt of ECSs are reported in [38]–[41].

Compared with capacitive sensors, ECSs are less sensitive to the surface conditions of the target and more sensitive to the electrical properties of the target, due to the penetration of the eddy currents in the target (the "skin" effect). The penetration depth δ of the eddy currents is defined by

$$\delta = \sqrt{\frac{\rho}{\pi f_{\text{exc}} \mu}} \tag{11}$$

where μ is the target permeability, ρ is its resistivity, and f_{exc} is the excitation frequency.

The penetration depth is defined as the depth at which the eddy current intensity drops down to ~37% (i.e., $1/e$) of its intensity at the target surface. Table II shows the penetration/skin depth in copper at different frequencies, together with the associated thermal drift due to the temperature dependence of the target conductivity.

When measuring very small displacements in the micrometer and nanometer range, a penetration depth of tens or even hundreds of micrometers creates a significant offset, even when

TABLE II
SKIN DEPTH AND THERMAL DRIFT DUE TO THE SKIN DEPTH VARIATION IN A COPPER TARGET

Excitation frequency	Skin depth in copper	Thermal drift (due to the temp. coefficient of the target conductivity)
1 MHz	66 μm	90 nm/K
20 MHz	15 μm	20 nm/K
200 MHz	4.7 μm	6 nm/K

the sensing coil is almost touching the target. This is because the position of the target is identified by the "center of density of the eddy currents," which is inside the target and not on its surface. This offset is one of the main sources of instability and the relatively low resolution associated with eddy current position sensors. Methods for simultaneously sensing the distance to the target, as well as the temperature of the target and the sensing coil, are reported [42]. These solutions can significantly improve the thermal stability of the sensor, but at the expense of a more complicated and power-hungry electronic interface. Using more power leads to additional heat generation and self-heating of the sensing coil, resulting in thermal gradients which might deteriorate the efficiency of this method.

Ways to improve sensitivity and reduce the instability introduced by the penetration depth are either to use a target with small resistivity (i.e., high conductivity), or increase the frequency of the magnetic field. Increasing the conductivity of the target means using special materials and/or special operating conditions (i.e., cryogenic temperatures), which is not very practical. Increasing the excitation frequency when using a typical densely wound coil (with or without a magnetic core) is problematic because of the low self-resonance frequency caused by the large value of the inductance, and the relatively large parasitic capacitance associated with the coil. Flat coils with fewer turns are preferred since their parasitic capacitance is quite limited. When operated at a higher frequency, these coils have a higher quality factor (due to the very low series resistance) and hence are less sensitive to interferences. Moreover, the flat structure of the coil makes it volume-efficient and provides improved mechanical stability [43].

B. Interface Electronics for ECSs

The presence of a conductive target in the vicinity of the sensing coil alters its impedance. The reason to consider the sensing coil as "impedance" rather than an inductance is related to the nonidealities of the practical coils mainly associated with the resistivity of the material used to produce the coils and the parasitic interwinding capacitance. The presence of the target has an impact on:

1) the equivalent inductance of the coil $L_s(L_p)$;
2) the losses in the sensing coil (the resistive part of the impedance—$R_s(R_p)$) and the quality factor Q;
3) on the value of the parasitic capacitance C, when the distance to the target is comparable with the pitch of a flat sensing coil.

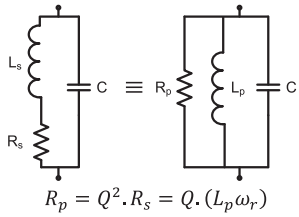

Fig. 16. Equivalent electric models of the sensing coil.

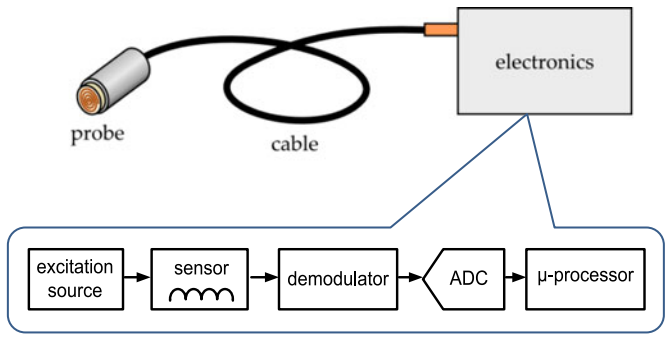

Fig. 17. Conventional architecture of an ECS interface.

Fig. 16 shows the two most frequently used lamped electrical models of the sensing coil, where ω_r is the resonance frequency and $L_p \sim L_s$.

Fig. 17 shows the conventional architecture of an ECS interface. The electronic interface is connected to the sensor via a cable with a length up to a few meters. This prevents the heat generated in the electronic box to heat up the sensor, and hence allows higher power consumption. The electronic interface measures the impedance of the sensing coil, which is normally dominated by its reactance X_L (the inductive component). This is achieved by applying an ac excitation signal (from an excitation source) to the sensing coil with a fixed frequency. The excitation signal can be a known voltage or current. What is measured is the current through, or the voltage drop over, the reactance X_L of the coil. The same method can be realized in an ac bridge configuration. A drawback to this kind of interface is power inefficiency.

Most of the available ECSs on the market operate following this principle. Table III shows some of the most advances custom off-the-shelf (COTS) eddy current displacement sensors.

The latest trends in the field of high performance ECSs for nano- and sub-nanometer displacement measurement show an increase in the excitation frequency in the MHz range. A higher excitation frequency provides not only higher sensitivity and lower thermal drift due to the reduced skin depth of the eddy currents in the target, but also a higher quality factor, providing better immunity to external interferences. Another trend is to integrate the readout electronics into the sensor head and to digitize the output signal, which will allow safe transmission of the measured result either via a long cable or wirelessly, and allows the creation of sensor networks. Operating at a high excitation frequency allows the use of flat air coils with low inductance, which, as already mentioned, can be mechanically very stable. However, employing a higher excitation frequency and lower

TABLE III
COTS NANOMETER RESOLUTION EDDY CURRENT DISPLACEMENT SENSORS

Supplier & Sensor	Nominal standoff (mm)	Range (mm)	Resolution (1kHz BW) (RMS, nm)	Thermal sensitivity (Nm/K)	Power (mW)
Kaman KD-5100	0.4	3.8	3.1	90	<2000
Blue line SFQ 600	1	0.8	21	100	700
*Baumer IPRM	0.8	1	80	10.000	<200
*μ/ε NCDT 3001	1.4	2	1.600	600	?

*Electronic interface integrated in the sensor head with voltage output.

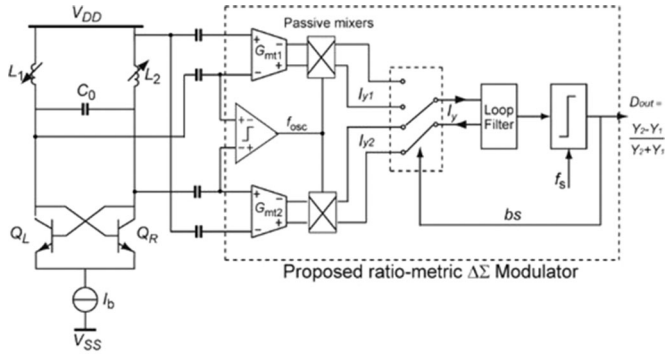

Fig. 18. Read-out circuit for an ECS-based displacement sensor with digital output (inductance-to-digital converter: IDC).

inductance of the sensing coil creates additional challenges to the interface electronics, especially for power efficiency. A preferred solution in this case is to boost the coil impedance by making it part of a parallel *LC*-resonator. Since at the resonance frequency the parallel *LC* network is open, the resonator impedance will be equal to $R_{\rm p}$ (see Fig. 16), which typically has a very high value and can be measured with considerably lower power consumption compared to the conventional approach presented in Fig. 17. In [6], a review is presented of the integrated ECS interfaces reported in the last decade which apply the resonator principle.

Recently, COTS-integrated inductance-to-digital converters were introduced to the market. An example is the LDCxxxx series from Texas Instruments.[1] The basic principle of operation employed is presented in [44]. The LDC1101 is an inductance-to-digital converter which can simultaneously measure the impedance and the resonant frequency of an external *LC* resonator comprised by the sensing coil and a reference capacitor, whereas the LDC1312/4 and LDC1612/4 measure only the resonant frequency of the resonator. By monitoring the amount of power injected into the resonator, the LDC1101 can determine the equivalent parallel resistance of the resonator R_p in the range from 1.25 to 90 kΩ. The resonant oscillation frequency f_r (up to 10 MHz) is measured by comparing it to the external reference frequency provided. The measured frequency can then be used to determine the inductance of the *LC* circuit.

The approach used in the LDCxxxx has the advantage of employing a simple and power-efficient demodulation technique, at the expense of lower sensitivity, as R_p is less sensitive to the displacement of the target than L_p, and $f_r \sim 1/\sqrt{L_p}$. Also, R_p is more sensitive to the temperature variation in the conductivity of the target.

A frontend resonator solution with a cross-coupled *LC* oscillator is proposed in [45]–[49]. The goal is to improve the performance of the ECS with respect to higher resolution, lower thermal drift, better long-term stability, and a smaller form factor, without compromising power efficiency. Achieving this will allow ECSs to be more competitive in the field of power-efficient displacement measurement in the nanometer and sub-nanometer ranges with applications such as: accelerometers, vibrometers, pressure sensors, inertial sensors, etc. Increasing the excitation frequency in the range of hundreds of MHz will allow the thickness of very thin conductive membranes to be measured [50].

For any precise measurement, using an accurate reference and an accurate method for comparison between the reference and the measurand is crucial. It is always beneficial if the reference is of the same nature as the measurand. In this sense, when measuring distance/displacement, the best reference is also distance/displacement. However, as the comparison must happen in the electrical domain after converting the sensed displacement into inductance change, the second best option is to compare the inductance of the sensor with a reference inductance. This is realized in the proposed architecture in Fig. 18 [47], which is similar to the architectures used in [45], [46], [48], and [49]. The reference inductance is included in the resonator loop. Physically, the reference inductor can be a "copy" of the sensing inductor preferably integrated into the sensor head. This allows two modes of operation: 1) differential mode when both flat coils L_1 and L_2 are used as sensors [45]–[47], and 2) normal mode when one of the coils is facing a fixed target (also integrated into the sensor head) at a nominal distance [48], [49].

Assuming the resonator has a high *Q*-factor, both coils experience the same loop current, as they are connected in series in the resonator. The interface circuit, after removing the carrier excitation frequency with the help of the G_m stages and the passive mixers, measures the voltages over the two inductors ratiometrically. In this way, the effect of the fluctuations and the noise of the loop current, generated mainly by the tail current I_b, are effectively cancelled, as they mainly cause a multiplicative error. The function $(L_1 - L_2)/L_1$ is realized in an oversampling sigma/delta ADC. The two channels delivering the voltage over the inductances to the input of the ADC (G_m plus the mixer) must be designed with maximum symmetry and very good linearity, to guarantee sufficient suppression of the correlated noise and drift of the oscillating frontend stage [51].

The ECS interface presented in [48] operates with a ∼126 MHz excitation frequency. It has a measurement range of 10 μm and a resolution of 0.6 nm (14.1-bit dynamic range). The signal bandwidth is 2 kHz and the power consumption is ∼20 mW. This chip is implemented in a 0.18-μm CMOS process.

[1][Online]. Available: http://www.ti.com/lsds/ti/sensing-products/inductive-sensing/inductive-sensing-overview.page

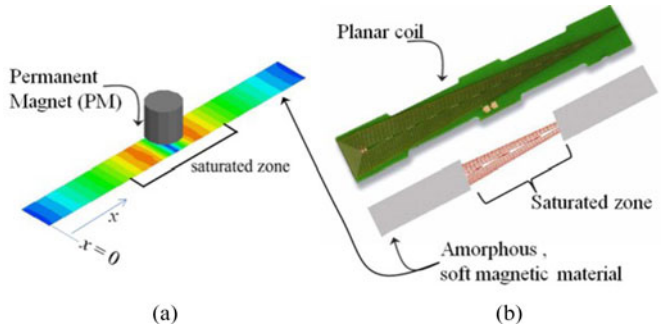

Fig. 19. Magneto-inductive position sensor. It uses (a) a PM and soft magnetic material, and (b) a planar coil, whose effective area is modulated depending on the position of the PM [52].

IV. Magnetic Displacement Sensors

Magnetic sensors have a well-established performance history in the linear and angular displacement-sensing domain, owing to features such as ruggedness and low power consumption. In comparison with the eddy current and capacitive sensors, magnetic sensors based on the semiconductor sensing elements discussed below are known to possess high sensitivity, wide range, high resolution, etc., despite their simple interfacing circuitries.

Based on the sensing mechanism, the magnetic displacement sensors can be broadly classified into two categories: 1) magneto-inductive (MI) [52], [53] and 2) magnetoresistance (MR) [54]–[56] or Hall Effect [56] type of sensors. Both use a permanent magnet (PM) to form a predefined magnetic field pattern, and differ only in the magnetic field sensing element employed. Other than the above-mentioned two categories, the sensors such as linear variable differential transformers, which work based on the change in the mutual inductance between the primary and secondary windings as function of the position of the magnetic core, are in use in industry. The technology is well known and mature. Hence, those are not included in this review.

In MI-type sensors, the permeability of the core, and hence inductance of the coil, is changed due to the measurand, while in the second type, the sensing elements based on the Hall effect or MR effect are used to measure the value of the field by the PM to compute the position/displacement. The details, designs, applications, and limitations of these types of sensors are discussed below.

A. Magneto-Inductive Position Sensors

Fig. 19 illustrates the internal structure and the idea behind a typical MI-type position sensor. As shown in Fig. 19(a), the position of the PM changes with respect to the linear position x. Here, x is the measurand. When the PM moves, the portion of thin, soft magnetic material underneath it becomes saturated [52]. A planar coil with a triangular shape, as shown in Fig. 19(b), is kept directly above this magnetic sheet. The inductance of the coil changes as a function of x as the coil has the triangular shape and the saturated zone that provides a very low relative permeability that moves along with the PM.

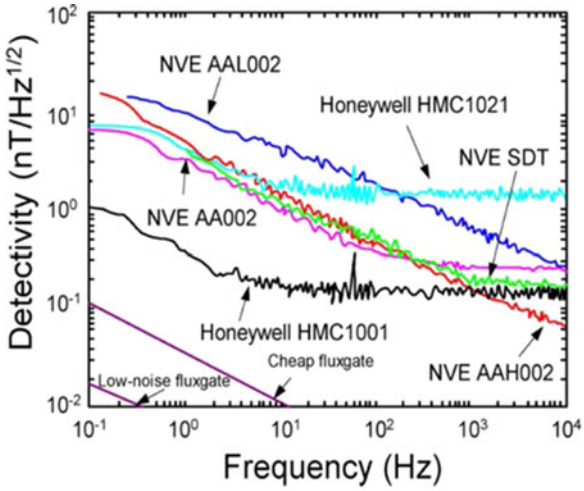

Fig. 20. Noise performance of various magnetic sensors [56]. NVE AAL002, NVE AA002, and NVE AAH002 are GMR-based sensors [62], while NVE SDT is a tunneling magnetoresistance (TMR) based sensor.

For such sensors, the inductance of the coil is measured using well-established oscillator circuits [52], [53], which are preferably in parallel resonance to keep the power requirement low. Linear MI-type position sensors with a range of 55 mm and resolution of 0.025% of full-scale (FS) are available in the market [53]. They have a typical frequency response in the range of 1 kHz and 0.025% FS temperature stability. The wear-free MI-type displacement sensor is a well-appreciated alternative for the inherently wear-prone potentiometer-type sensor. More research in the direction of 1) producing PMs with a high ratio of flux density to weight, and 2) developing soft magnetic materials with very low hysteresis and less sensitivity to temperature, etc., will help to further improve the performance and applications of the MI sensors.

B. Magnetoresistance or Hall Effect Based Position Sensors

Over the last two decades, significant improvements have been made in the domain of magnetic field sensing. This is primarily due to developments in the Hall effect, giant MR (GMR) [54], [55] and anisotropic MR (AMR) [56], [57] based technologies, which have had a noticeable impact on the magnetic field sensing and the associated application sector.

The performance of Hall effect, GMR, and AMR magnetic field sensors, in terms of sensitivity, noise, and bandwidth verses power requirement, size of the sensor and cost, is several steps ahead of other existing techniques [55]. A comparative noise performance for various existing techniques has been reported. It is reproduced from [56] and shown in Fig. 20. As can be seen from Fig. 20, although MR-type sensors have higher noise than, say, low-noise fluxgate sensors, they are comparatively quite small in size and low in cost. Due to these benefits, these technologies have helped various research groups and industries to develop efficient linear and angular displacement measurement sensors [58]–[61]. For example, high accuracy angular position

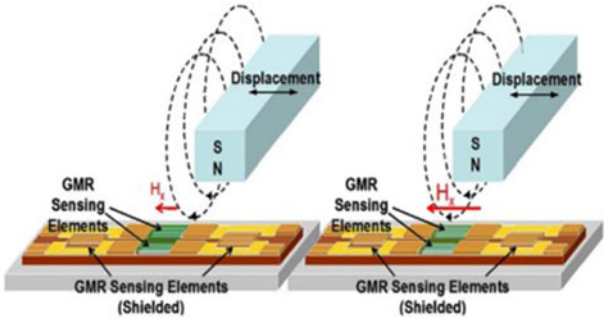

Fig. 21. GMR-based sensor for nanopositioning [54].

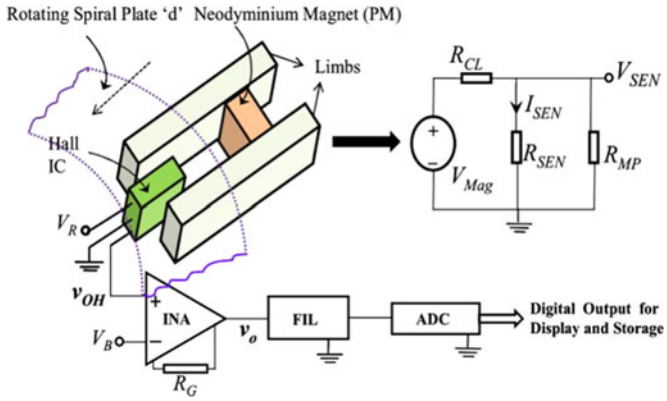

Fig. 22. Variable reluctance Hall effect angle sensor [60]. An electrical analogy is also shown. R_{MP} corresponds to the reluctance of the path through the moving part, while R_{SEN} and R_{CL} represent the reluctance of the section of path through the Hall sensor and the section of path through the limb.

sensing with nanodegree accuracy has been developed using a multisensor approach and is reported in [61].

1) Linear Position Sensing Using MR Sensors: The impact of GMR- and TMR-based read head technologies in the growth of the magnetic hard disk drive (HDD) is well known [63]. These heads primarily enabled to realize a very high data rate for writing and reading, which has led to today's low cost, reliable HDDs. Features such as high sensitivity, bandwidth, and signal-to-noise ratio, as well as a lightweight MR head, enable ultrafast positioning and reading of data [64].

Fig. 21 shows the idea behind a nanoposition sensor using a combination of a PM and GMR sensor. This sensor, along with appropriate feedback techniques, is used to realize nanopositioning systems [65] with a high bandwidth [54] for lithography tools and semiconductor inspection systems, molecular biology, nanofabrication and manufacturing, etc. The scheme presented in [54] has nanometer-scale precision control at dimensions below 100 nm.

Similar MR/Hall effect sensor-based approaches for sensing angular position have been reported in [66]. This sensor employs two sets of compact Hall effect-based sensors and two semi-ring-shaped PMs. The magnetic field seen by the Hall sensors changes as a function of the angle being measured. A ratio-metric computation is performed to obtain the final output, which is expected to have very low sensitivity to dust, moisture, vibration, etc. Although the system is simple and the signal conditioning required is very small, the presence of any other magnetic object in the vicinity of the magnetic field of the PM and Hall ICs will introduce errors. This issue could be solved using appropriate magnetic shielding, but this is an expensive solution. The precision ($\pm$6 deg) reported for the prototype is not sufficient for many practical applications.

2) Variable Reluctance Hall Effect Sensors: Variable reluctance position sensors have very good sensitivity, but they require relatively large moving parts with nonstandard shapes and windings [67], [68]. To measure the magnetic field, instead of the windings, a Hall effect based sensor illustrated in Fig. 22 could be used [60]. In this case, a flux path is present through the limbs and the field is sensed using a Hall effect sensor. This field becomes modified when a spiral-shaped magnetic core is moved with respect to the angle, above the limbs. If the Hall effect sensor is placed in an optimal position, a linear output can be obtained for a range of 220 deg without complex signal conditioning [69]. Resolution of the system is limited by the manufacturing precision of the moving part and misalignments. Factors such as aging of the PM and temperature sensitivity of the Hall sensors also need attention, especially for high-resolution applications. Later, an improved approach was reported which uses a similar design, but the moving parts are made of standard circular shapes that are easy to manufacture and hence the precision requirement for the periphery is not a constraint. Power requirements for these types of systems are low as no electrical signal is used for the magnetic field excitation, and power is required only for the Hall ICs and a couple of instrumentation amplifiers and opamps. The designs in [59] and [60] are useful for developing brake-ware monitoring sensors.

Hall effect based angular sensing solutions are required to estimate the rotor position of the permanent-magnet synchronous motor (PMSM). It has been reported that the Hall effect sensor based approach achieves a strong antitemperature drift performance [70]. In addition, the Hall effect-based sensors are small in size and lightweight, which is very useful in PMSM applications where strict space and weight requirements exist [70].

Inclination is another important parameter that is of interest in the industrial sensing domain. A novel magnetic sensor configuration suitable for inclination measurement has been reported recently in [71]. A diagram of the same configuration is shown in Fig. 23. In this case, a ferrofluid is employed which flows through two nonmagnetic tubes and takes a predefined shape, depending on the inclination. As the ends of the ferrofluid are connected to two PMs, the field seen by the Hall effect IC varies as a function of the inclination. The electronics required to obtain a useful output is simple, but the working range is limited to less than 15 deg [71].

C. Magnetic Sensors for Enhancing the Performance of Navigation

The range of the linear position sensing systems so far discussed above is limited to a few cm, while in certain applications the range as well as coverage area/volume needs to be quite large

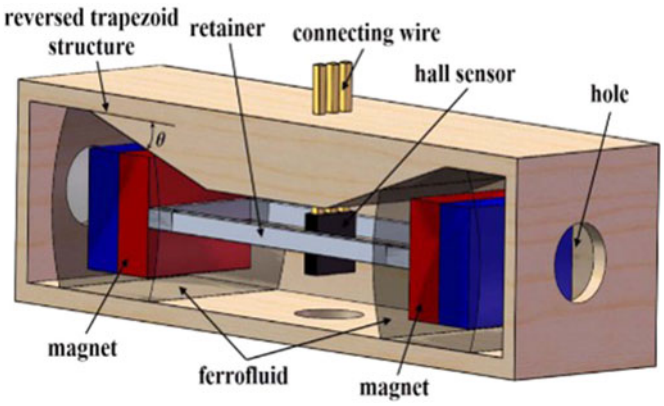

Fig. 23. Ferrofluid and Hall effect sensor-based inclinometer [71].

TABLE IV
CHARACTERISTICS OF THE DISPLACEMENT SENSORS

Parameter	Capacitive sensor	ECS	M-I, Hall, MR, etc.
Compact structure	yes	Yes (flat coil)	yes
Mechanical stability	yes	Yes (flat coil)	yes
Sensitivity to environment	yes	limited	low
Sensitivity to target surface	yes	no	no
Sensitivity to target bulk	no	yes	yes
Sensitivity to tilt	yes	yes	yes
Need for alignment	yes	yes	yes
Sensitivity to external magnetic fields	no	Limited (if $f\uparrow$)	appropriate shield is required
Sensitivity to external electric fields	limited	no	no
Linear/Nonlinear transfer characteristic	both available	Nonlinear	both available
Electrical excitation of sensors is required	yes	yes	no, permanent magnet can be used
Complexity level of interfacing schemes	moderate	moderate	low

for, say, tracking a person or object in a battle field or factory. One of the obvious choices is to use the global positioning system (GPS), but it may suffer due to the limited coverage area, blind spot, errors due to clock drift or clock offset on board the satellite, errors due to altered travel time of GPS satellite signal by atmospheric effect, etc. An interesting approach of indoor navigation, with the help of foot-mounted inertial navigation and magnetic sensors, after the GPS signal is lost is presented in [72]. The system in [72] uses an MEMS inertial measurement unit (IMU), in combination with a magnetometer that provides the value of the earth's magnetic field to estimate the heading, with the help of a gravity vector resolved using two orthogonal accelerometers. In this case, the magnetic field data are effectively used to improve the accuracy of the overall system. The approach presented is quite practical and the cost and the size of the IMU, power requirement for the entire unit, etc., are low enough for the applications envisaged in [72]. A similar approach has been developed and reported in [73]. For certain applications, the system still needs improvement in terms of accuracy as it showed 16 m of position error while tested for a trajectory of about 1 km. For some of the industrial applications, an electromagnetic-based navigation that enhances the accuracy and resolution is useful [74]. An inspection vehicle that uses the gradient of the magnetic field of an overhead current carrying cable for navigation has been reported in [74]. This approach could give millimeter-level navigation accuracy.

V. DISCUSSION

A brief note on the displacement sensors based on capacitive, eddy current, and some of the relatively new magnetic sensing approach is presented in Table IV. The parameters for comparison are selected based on the common features of the types of the sensors that are of practical importance. The data provided in Table IV will be useful for engineers to select the appropriate type depending on the applications and constrains.

VI. CONCLUSION

A comprehensive review of the recently reported advances in the field of capacitive, eddy current, and magnetic displacement sensing was presented in this paper. The position sensors using the above-mentioned principles have numerous applications in industry, ranging from nanopositioning systems for micro- or nanofabrication, high bandwidth and high resolution SEM imaging systems, and high density data storage systems to industrial automotive, navigation applications. Even though the sensor design is important, the associated interfacing electronics/circuitry played a key role in the overall performance of the sensor system. Thus, special attention was given to the interface electronics section, while conducting the review. This review paper will allow researchers to identify the important gaps and work toward advancing displacement sensor technology. Similarly, it will be useful for sensor design and application engineers in the sector to make the best design choices, as the most recent developments in this domain can be easily taken from this paper.

REFERENCES

[1] T. R. Hicks and P. D. Atherton, *The Nano Positioning Book: Moving and Measuring to Better Than a Nanometer*. Arlington, VA, USA: ISTE, 2000.
[2] S. Nihtianov, "Measuring in the sub-nanometer range: Capacitive and Eddy current nano-displacement sensors," *IEEE Ind. Electron. Mag.*, vol. 8, no. 1, pp. 6–15, Mar. 2014.
[3] L. K. Baxter, *Capacitive Sensors: Design and Applications*. New York, NY, USA: IEEE, 1997.
[4] W. Bracke, R. Puers, and C. Van Hoof, *Ultra-Low Power Capacitive Sensor Interfaces*. New York, NY, USA: Springer, 2007.
[5] M. A. P. Pertijs and Z. Tan, "Energy-efficient capacitive sensor interfaces," in *Nyquist AD Converters, Sensor Interfaces, and Robustness*. New York, NY, USA: Springer, 2013, pp. 129–147.
[6] M. R. Nabavi and S. Nihtianov, "Design strategies for eddy current displacement sensor systems: Review and recommendations," *IEEE Sens. J.*, vol. 12, no. 12, pp. 3346–3355, Dec. 2012.
[7] S. D. Roach, "Designing and building an eddy current position sensor," *Sensors, J. Appl. Sens. Technol.*, vol. 15, no. 9, pp. 56–74, 1998.
[8] C. Huai-Ning *et al.*, "An investigation of micro-weighing with an eddy current transducer," *Rev. Sci. Instrum.*, vol. 59, no. 10, pp. 2297–2299, Oct. 1988.

[9] P. Vasseur and A. Billat, "Contribution to the development of a smart sensor using eddy currents for measurement of displacement," *Meas. Sci. Technol.*, vol. 5, pp. 889–895, 1994.

[10] T. Hitz and S. D. Welsby, "True position measurement with eddy current technology," *Sensors*, vol. 14, no. 11, pp. 30–40, 1997.

[11] Y. Yating, D. Pingan, and W. Zhenwei, "Study on the electromagnetic properties of eddy current sensor," in *Proc. IEEE Int. Conf. Mechatron. Autom.*, vol. 4, 2005, pp. 1970–1975.

[12] S. Fericean and R. Droxler, "New noncontacting inductive analog proximity and inductive linear displacement sensors for industrial automation," *IEEE Sens. J.*, vol. 7, no. 11, pp. 1538–1545, Nov. 2007.

[13] K. Banerjee, B. Dam, and K. Majumdar, "A novel FPGA-based LVDT signal conditioner," in *Proc. IEEE Int. Symp. Ind. Electron.*, 2013, pp. 1–6.

[14] G. Chen, B. Zhang, P. Liu, and H. Ding, "An adaptive analog circuit for LVDT's nanometer measurement without losing sensitivity and range," *IEEE Sens. J.*, vol. 15, no. 4, pp. 2248–2254, Apr. 2015.

[15] H. U. Meyer, "An integrated capacitive position sensor," *IEEE Trans. Instrum. Meas.*, vol. 45, no. 2, pp. 521–525, Apr. 1996.

[16] M. Gasulla, X. Li, G. C. M. Meijer, L. Van derHam, and J. O W. Spronck, "A contactless capacitive angular-position sensor," *IEEE Sens. J.*, vol. 3, no. 5, pp. 607–614, Oct. 2003.

[17] A. A. Kuijpers, R. J. Wiegerink, G. J. M. Krijnen, T. S. J. Lammerink, and M. Elwenspoek, "Capacitive long-range position sensor for microactuators," in *Proc. 17th IEEE Int. Conf. Micro Electro Mech. Syst.*, 2004, pp. 544–547.

[18] F. Toth and G. C. M. Meijer, "A low-cost, smart capacitive position sensor," *IEEE Trans. Instrum. Meas.*, vol. 44, no. 3, pp. 768–770, Jun. 1995.

[19] B. B. Boser and R. T. Howe, "Surface micromachined accelerometers," *IEEE J. Solid-State Circuits*, vol. 31, no. 3, pp. 366–375, Mar. 1996.

[20] J. Lee, X. Huang, and P. B. Chu, "Nano precision MEMS capacitive sensor for linear and rotational positioning," *J. Microelectromech. Syst.*, vol. 18, no. 3. pp. 660–670, 2009.

[21] V. P. Petkov, G. K. Balachandran, and J. Beintner, "A fully differential charge-balanced accelerometer for electronic stability control," *IEEE J. Solid-State Circuits*, vol. 49, no. 1, pp. 262–270, Jan. 2014.

[22] M. Lemkin and B. E. Boser, "A three-axis micromachined accelerometer with a CMOS position-sense interface and digital offset-trim electronics," *IEEE J. Solid-State Circuits*, vol. 34, no. 4, pp. 456–468, Apr. 1999.

[23] Z. Tan, "Energy-efficient capacitive-sensor interfaces," Ph.D. dissertation, Electron. Instrumentation Laboratory, Delft Univ. Technol., Delft, The Netherlands, 2013.

[24] M. Paavola, M. Kamarainen, J. A. M. Jarvinen, M. Saukoski, M. Laiho, and K. A. I. Halonen, "A micropower interface ASIC for a capacitive 3-axis micro-accelerometer," *IEEE J. Solid-State Circuits*, vol. 42, no. 12, pp. 2651–2665, Dec. 2007.

[25] B. V. Amini and F. Ayazi, "A 2.5-V 14-bit $\sigma\delta$ CMOS SOI capacitive accelerometer," *IEEE J. Solid-State Circuits*, vol. 39, no. 12, pp. 2467–2476, Dec. 2004.

[26] A. Baschirotto *et al.*, "A$\pm$1-g dual-axis linear accelerometer in a standard 0.5-μm CMOS technology for high-sensitivity applications," *IEEE J. Solid-State Circuits*, vol. 38, no. 7, pp. 1292–1297, Jul. 2003.

[27] A. Heidary and G. C. M. Meijer, "Features and design constraints for an optimized SC front-end circuit for capacitive sensors with a wide dynamic range," *IEEE J. Solid-State Circuits*, vol. 43, no. 7, pp. 1609–1616, Jul. 2008.

[28] Z. Tan, S. H. Shalmany, G. C. M. Meijer, and M. A. P. Pertijs, "An energy-efficient 15-bit capacitive-sensor interface based on period modulation," *IEEE J. Solid-State Circuits*, vol. 47, no. 7, pp. 1703–1711, Jul. 2012.

[29] F. Krummenacher, "A high-resolution capacitance-to-frequency converter," *IEEE J. Solid-State Circuits*, vol. SC-20, no. 3, pp. 666–670, Jun. 1985.

[30] P. Bruschi, N. Nizza, and M. Piotto, "A current-mode, dual slope, integrated capacitance-to-pulse duration converter," *IEEE J. Solid-State Circuits*, vol. 42, no. 9, pp. 1884–1891, Sep. 2007.

[31] P. Bruschi, N. Nizza, and M. Dei, "A low-power capacitance to pulse width converter for MEMS interfacing," in *Proc. 34th Eur. Solid-State Circuits Conf.*, 2008, pp. 446–449.

[32] Z. Tan, R. Daamen, A. Humbert, Y. V. Ponomarev, Y. Chae, and M. A. P. Pertijs, "A 1.2-V 8.3-nJ CMOS humidity sensor for RFID applications," *IEEE J. Solid-State Circuits*, vol. 48, no. 10, pp. 2469–2477, Oct. 2013.

[33] Z. Tan *et al.*, "A 1.8 V 11μW CMOS smart humidity sensor for RFID sensing applications," in *Proc. IEEE Asian Solid State Circuits Conf.*, 2011, pp. 105–108.

[34] S. Oh *et al.*, "A dual-slope capacitance-to-digital converter integrated in an implantable pressure-sensing system," *IEEE J. Solid-State Circuits*, vol. 50, no. 7, pp. 1581–1591, Jul. 2015.

[35] H. Omran, M. Arsalan, and K. N. Salama, "A robust parasitic-insensitive successive approximation capacitance-to-digital converter," in *Proc. IEEE Custom Integr. Circuits Conf.*, 2014, pp. 1–4.

[36] A. Alhoshany, H. Omran, and K. N. Salama, "A 45.8 fJ/Step, energy-efficient, differential SAR capacitance-to-digital converter for capacitive pressure sensing," *Sens. Actuators A, Phys.*, vol. 245, pp. 10–18, 2016.

[37] S. Xia, K. Makinwa, and S. Nihtianov, "A capacitance-to-digital converter for displacement sensing with 17b resolution and 20μs conversion time," in *Proc. IEEE Int. Solid-State Circuits Conf.*, 2012, pp. 198–200.

[38] L. Yang, X. Shenga, M. Lianb, and Y. Wang, "Influence of tilt angle on eddy current displacement measurement," *J. Nondestructive Test. Eval.*, vol. 31, no. 4, pp. 289–302, 2016.

[39] T. Theodoros, "Analytical model for tilted coils in eddy-current nondestructive inspection," *IEEE Trans. Magn.*, vol. 41, no. 9, pp. 2447–2454, Sep. 2005.

[40] Y. Le Bihana, "Lift-off and tilt efects on eddy current sensor measurements: A 3-D finite element study," *Eur. Phys. J. Appl. Phys.*, vol. 17, pp. 25–28, 2002.

[41] J. Vogel and S. Nithianov, "Tilt sensitivity of an eddy-current position sensor for high-precision applications," in *Proc. Euspen'16 Int. Conf. Exhib.*, Nottingham, U.K., May 2016, pp. 177–178.

[42] H. Wang and Z. Feng, "Ultrastable and highly sensitive eddy current displacement sensor using self-temperature compensation," *Sens. Actuators A, Phys.*, vol. 203, no. 1, pp. 362–368, Dec. 2013.

[43] J. Vogel and S. Nihtianov, "Study of the self-resonance frequency of a flat coil for an eddy-current position sensor," in *Proc. IEEE Sens. Conf.*, Orlando, USA, Oct./Nov. 2016, pp. 1–3.

[44] *Resonant Inductive Sensing With Algorithmic Control Loop for Tuning Negative Impedance to Resonator Impedance*, U.S. Patent 2016/0195598 A1, Jul. 7, 2016.

[45] M. R. Nabavi and S. Nihtianov, "Eddy current sensor interface for advanced industrial applications," *IEEE Trans. Ind. Electron.*, vol. 58, no. 4, pp. 4414–4423, Sep. 2011.

[46] M. R. Nabavi, M. A. P. Pertijs, and S. Nihtianov, "An interface for eddy current displacement sensors with 15-bit resolution and 20 MHz excitation," in *Proc. IEEE Eur. Solid State Circuits Conf.*, Sep. 2010, pp. 290–293

[47] A. Fekri, M. Reza Nabavi, N. Radeljić-Jakić, Z. Chang, M. Pertijs, and S. Nihtianov, "An eddy-current displacement-to-digital converter based on a ratio-metric delta-sigma ADC," in *Proc. Eur. Solid State Circuits Conf.*, Venice, Italy, Sep. 2014, pp. 403–406.

[48] V. Chaturvedi, K. Makinwa, and S. Nihtianov, "A 0.6 nm resolution 19.8 mW eddy-current displacement sensor interface with 126 MHz excitation," in *Proc. IEEE Int. Solid-State Circuits Conf.*, Feb. 2017, pp. 174–175.

[49] V. Chaturvedi, J. G. Vogel, K. A. A. Makinwa, and S. Nihtianov, "A 9.1 mW inductive displacement-to-digital converter with 1.85 nm resolution," in *Proc. Symp. VLSI Technol. Circuits*, Kyoto, Japan, Jun. 2017, pp. C80–C81.

[50] W. Li, Y. Ye, K. Zhang, and Z. Feng, "A thickness measurement system for metal films based on eddy-current method with phase detection," *IEEE Trans. Ind. Electron.*, vol. 64, no. 5, pp. 3940–3949, May 2017.

[51] V. Chaturvedi, J. Vogel, and S. Nihtianov, "Suppression efficiency of the correlated-noise and drift of self-oscillating pseudo-differential eddy current displacement sensor," in *Proc. 30th Eurosens. Conf.*, Budapest, Hungary, Sep. 2016, pp. 946–949.

[52] M. Jagiella, S. Fericean, R. Droxler, and R. Dorneich, "New magneto-inductive sensing principle and its implementation in sensors for industrial applications," in *Proc. IEEE Sens.*, 2004, pp. 1020–1023.

[53] "Magneto-inductive displacement sensors," Ortenburg, Germany. [online]. Available: http://www.micro-epsilon.com/download/products/cat–mainSENSOR–en-us.pdf, accessed on Aug. 18, 2017.

[54] V. Kartik, A. Sebastian, T. Tuma, A. Pantazi, H. Pozidis, and D. R. Sahoo, "High-bandwidth nanopositioner with magnetoresistance based position sensing," *Mechatronics*, vol. 22, no. 3, pp. 295–301, 2012.

[55] E. Eleftheriou, "Nanopositioning for storage applications," *Annu. Rev. Control*, vol. 36, no. 2, pp. 244–254, 2012.

[56] P. Ripka and M. Janosek, "Advances in magnetic field sensors," *IEEE Sens. J.*, vol. 10, no. 6, pp. 1108–1116, Jun. 2010.

[57] R. Caruso, J. Michael, T. Bratland, C. H. Smith, and Schneider, "A new perspective on magnetic field sensing," *Sensors*, vol. 15, pp. 34–47, 1998.

[58] M. M. Miller *et al.*, "Development of a high precision absolute linear displacement sensor utilizing GMR spin-valves," *IEEE Trans. Magn.*, vol. 33, no. 5, pp. 3388–3390, Sep. 1997.
[59] A. C. Sreekantan and B. George, "A linearizing digitizer for differential sensors with polynomial characteristics," *IEEE Trans. Instrum. Meas.*, vol. 63, no. 5, pp. 1022–1031, May 2014.
[60] C. S. Anoop and B. George, "A new variable reluctance-hall effect based angle sensor," in *Proc. Int. Conf. Sens. Technol.*, 2012, pp. 454–459.
[61] S. Foong, K. M. Lee, and K. Bai, "Harnessing embedded magnetic fields for angular sensing with nanodegree accuracy," *IEEE/ASME Trans. Mechatron.*, vol. 17, no. 4, pp. 687–696, Aug. 2012.
[62] "Analog Sensors Catalog, AA and AB series: Datasheet," NVE Corporation, Eden Prairie, MN, USA, 2013, pp. 12–27.
[63] E. Grochowski, "Emerging trends in data storage on magnetic hard disk drives," Datatech (Sep. 1998), ICG Publ., 1998, pp. 11–16.
[64] E. E. Fullerton and J. R. Childress, "Spintronics, magnetoresistive heads, and the emergence of the digital world," *Proc. IEEE*, vol. 104, no. 10, pp. 1787–1795, Oct. 2016.
[65] T. J. Joseph and V. Kartik, "Nanometer resolution dynamic displacement measurement in industrial / high noise environments," in *Proc. IEEE Int. Conf. Ind. Technol.*, Mar. 2016, pp. 673–678.
[66] Y. Y. Lee, R. H. Wu, and S. T. Xu, "Applications of linear hall-effect sensors on angular measurement," in *Proc. IEEE Int. Conf. Control Appl.*, 2011, pp. 479–482.
[67] K. C. Kim, S. J. Hwang, K. Y. Sung, and Y. Kim, "A study on the fault diagnosis analysis of variable reluctance resolver for electric vehicle," in *Proc. IEEE Sens.*, 2010, pp. 290–295.
[68] Q. Tang, D. Peng, L. Wu, and X. Chen, "An inductive angular displacement sensor based on planar coil and contrate rotor," *IEEE Sens. J.*, vol. 15, no. 7, pp. 3947–3954, Jul. 2015.
[69] C. S. Anoop and B. George, "Study of a hall effect brake wear sensor using finite element modelling and analysis," in *Proc. 19th IMEKO TC-4 Symp. Meas. Electr. Quantities*, Barcelona, Spain, Jul. 2013, pp. 480–484.
[70] H. U. Jianhui, J. Zou, F. Xu, Y. Li, and Y. Fu, "An improved PMSM rotor position sensor based on linear hall sensors," *IEEE Trans. Magn.*, vol. 48, no. 11, pp. 3591–3594, Nov. 2012.
[71] J. Yao, S. Liu, Z. Li, and D. Li, "A novel ferrofluid inclinometer exploiting a hall element," *IEEE Sens. J.*, vol. 16, no. 22, pp. 7986–7991, Nov. 2016.
[72] J. Bird and D. Arden, "Indoor navigation with foot-mounted strapdown inertial navigation and magnetic sensors [Emerging opportunities for localization and tracking]," *IEEE Wireless Commun.*, vol. 18, no. 2, pp. 28–35, Apr. 2011.
[73] M. H. Afzal, V. Renaudin, and G. Lachapelle, "Use of earth's magnetic field for mitigating gyroscope errors regardless of magnetic perturbation," *Sensors*, vol. 11, no. 12, pp. 11390–11414, Nov. 2011.
[74] M. Zhang, S. W. Or, S. Wang, and F. Chang, "Electromagnetic navigation linear displacement transducer based on magnetic field gradient technique," *IEEE Trans. Magn.*, vol. 51, no. 11, Nov. 2015, Art. no. 8003204.

Boby George (M'07) was born in Kerala, India, in 1977. He received the M.Tech. and Ph.D. degrees in electrical engineering from the Indian Institute of Technology (IIT) Madras, Chennai, India, in 2003 and 2007, respectively.

He was a Postdoctoral Fellow with the Institute of Electrical Measurement and Measurement Signal Processing, Technical University of Graz, Graz, Austria, from 2007 to 2010. In 2010, he joined the faculty of the Department of Electrical Engineering, IIT Madras, where he is currently an Associate Professor. His areas of research interests include sensors and electronic instrumentation.

Dr. George is an associate editor for the IEEE SENSORS JOURNAL.

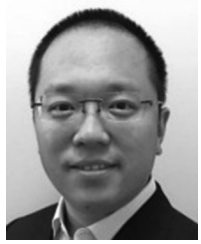

Zhichao Tan (S'09–M'13) received the B.Eng. degree from Xi'an Jiaotong University, Xi'an, China, in 2004, the M.Eng. degree from Peking University, Beijing, China, in 2008, and the Ph.D. degree from Delft University of Technology, Delft, The Netherlands, in 2013, all in electrical engineering.

Since June 2013, he has been with Analog Devices Inc., Wilmington, MA, USA, where he is currently a Staff IC Design Engineer. He has authored and coauthored 2 book chapters, 2 patents, and 15 technical journal and conference papers.

Dr. Tan is currently an associate editor for the IEEE TRANSACTIONS ON CIRCUITS AND SYSTEMS – I: REGULAR PAPERS and the IEEE SENSORS JOURNAL. He is also a member of the Technical Program Committee of the IEEE Asian Solid-State Circuits Conference and the IEEE Sensors Conference. He received two times the IEEE Solid-State Circuits Society Student Travel Grant Award.

Stoyan Nihtianov (M'93–SM'98) received the M.Sc. and Ph.D. degrees in electronics from the Technical University, Sofia, Bulgaria, in 1980 and 1987, respectively.

He is a Senior Research Fellow with the high-tech company ASML, The Netherlands. He is also a part-time Professor with the Electronics Instrumentation Lab, TU Delft, The Netherlands. He has authored or co-authored two books and three book chapters, more than 130 peer-reviewed journal and conference scientific papers in the field of sensors and sensor interface electronics. He holds 21 patents.

Prof. Nihtianov served as the Chair of the technical committee on MEMS@Nanotechnology of the Industrial Electronics Society (2013–2014). He is an AdCom member of the IEEE Industrial Electronics Society. He is also an associate editor for the IEEE TRANSACTIONS ON INDUSTRIAL ELECTRONICS and a Topical Editor for the IEEE SENSORS JOURNAL (Sensors Interface Electronics). He has been multiple times a member of the technical program committees of the IES flagship conferences: IECON, ISIE, and ICIT.